

Article

Study on the Effect of Post-Freezing Mechanical Properties of Polypropylene Fibre Concrete Based on BAS-BPNN

Cundong Xu ^{1,2}, Jun Cao ^{1,*} , Jiahao Chen ¹, Zhihang Wang ¹ and Wenhao Han ¹

¹ School of Water Conservancy, North China University of Water Resources and Electric Power, Zhengzhou 450046, China; xcundong@126.com (C.X.); cj13103198018@outlook.com (J.C.); cao13103198018@outlook.com (Z.W.); cj992766241@gmail.com (W.H.)

² School of Water Conservancy and Environmental Engineering, Zhejiang University of Water Resources and Electric Power, Hangzhou 310018, China

* Correspondence: cj992766241@163.com; Tel.: +86-13103198018

Abstract: An indoor accelerated freezing and thawing test of polypropylene fibre-reinforced concrete in chloride and sulphate environments was conducted using the “fast-freezing method” with the objective of investigating the damage law of the post-freezing mechanical properties of hydraulic concrete structures and studying the effects of different mixing amounts of polypropylene fibres on the mechanical properties of concrete. Furthermore, in order to reduce the cost of concrete tests and shorten the time required for conducting concrete tests, a backpropagation neural network based on a Beetle Antenna Search algorithm (BAS-BPNN) was established to simulate and predict the mechanical properties of polypropylene fibre-reinforced concrete. The accuracy of the model was verified. The results indicate that the order of improvement in the macro-physical properties of concrete due to fibre doping is as follows: PPF1.2 exhibited the greatest improvement in macro-physical properties of concrete, followed by PPF0.9, PPF1.5, PPF0.6, and PC. When the freezing and thawing medium and the number of cycles are identical, all four assessment indexes ($R2$, $RMSE$, SI , $MAPE$) demonstrate that the four groups of polypropylene fibre concrete exhibit superior performance to the control group of ordinary concrete. This indicates that polypropylene fibre can enhance the mechanical properties and freezing resistance of the concrete matrix, delay the process of freezing and thawing damage to the matrix, and extend the lifespan of the matrix, yet cannot prevent the ultimate failure of the matrix. The application of intelligent algorithms to optimise the parameters of an artificial neural network model can enhance its capacity to generalise and predict the mechanical properties of concrete. In terms of the coefficient of determination ($R2$), the Beetle Antenna Search algorithm (0.9782) outperforms the Particle Swarm Optimization (PSO; 0.9676), the Genetic Algorithm (GA; 0.9645), and the backpropagation neural network (BPNN; 0.9460). The improved backpropagation neural network based on the Beetle Antenna Search algorithm not only avoids the trap of local optimality but also improves the model accuracy while further accelerating the convergence speed. This approach can address the complexity, non-linearity, and modelling difficulties encountered during the freezing process of concrete. Moreover, it offers relatively accurate prediction outcomes at a reduced cost in comparison to traditional experimental methodologies.

Keywords: polypropylene fibre; concrete; freeze–thaw; chloride; sulphate free; neural network; beetle antennae search algorithm



Citation: Xu, C.; Cao, J.; Chen, J.; Wang, Z.; Han, W. Study on the Effect of Post-Freezing Mechanical Properties of Polypropylene Fibre Concrete Based on BAS-BPNN. *Buildings* **2024**, *14*, 1289. <https://doi.org/10.3390/buildings14051289>

Academic Editor: Flavio Stochino

Received: 29 March 2024

Revised: 24 April 2024

Accepted: 26 April 2024

Published: 2 May 2024



Copyright: © 2024 by the authors. Licensee MDPI, Basel, Switzerland. This article is an open access article distributed under the terms and conditions of the Creative Commons Attribution (CC BY) license (<https://creativecommons.org/licenses/by/4.0/>).

1. Introduction

Concrete materials are commonly used in engineering, but their application is limited due to brittleness, low tensile strength, and poor crack resistance. Northwest China's extreme environment and severe winter climate, coupled with soil and water rich in sulphate and chloride ions, subject the region's concrete buildings to salt ion erosion and freeze–thaw cycle damage. Therefore, it is necessary to conduct relevant research to

enhance the durability, freezing resistance, and safety of hydraulic buildings in extreme environments, including their service life. The indoor accelerated test for salt freezing and thawing cycles has demonstrated that concrete buildings are susceptible to salt-freezing coupling erosion, which can cause significant damage to the matrix material and structure. The mechanical properties of concrete and its frost resistance in chloride and sulphate environments decline noticeably with an increase in the number of freezing and thawing cycles. This decline is accompanied by an aggravation of the degree of damage to the concrete structure, causing the surface to gradually shrink and the resistance to cracking to be significantly reduced [1–3].

Recent studies have shown that adding various discontinuous fibres during the concrete preparation process can effectively improve its natural defects. Meanwhile, artificial fibres are more commonly used than natural fibres to inhibit concrete cracks and enhance its mechanical properties due to their high strength and low water absorption. Polypropylene fibre has superior performance due to its relatively uniform distribution in the matrix, simple production process, and low cost. A large number of tests have proved that the appropriate amount of addition can enhance the bond strength of the matrix interface within the concrete. Therefore, when preparing concrete, mixing it with polypropylene fibres is recommended. It is important to study the effect of polypropylene fibres on the mechanical properties of concrete, its anti-freezing properties, and its degradation due to salt freezing and thawing damage in concrete structures.

The addition of polypropylene fibres to concrete can significantly enhance the durability and dimensional stability of specimens [4]. Numerous experiments have demonstrated that this addition also improves the compressive strength, flexural strength, and modulus of elasticity of concrete [5–7]. At the microscopic level, studies have shown that the addition of polypropylene fibres reduces the porosity of concrete and improves its microstructural properties. This enhances the mechanical properties of concrete [8,9]. Polypropylene fibres can prevent the development of cracks in concrete when subjected to external forces [10–13]. Even after multiple freeze–thaw cycles, polypropylene fibres maintain the integrity of the concrete. Additionally, their low water absorption allows for better integration with the concrete, limiting the movement of salt ions and water in the matrix. The addition of polypropylene fibres has been shown to reduce the porosity of concrete, improving its microstructural properties and enhancing its mechanical properties [8,9]. Additionally, the inclusion of these fibres effectively enhances the impermeability of the concrete and its resistance to frost [14–19]. It is important to note that all evaluations presented here are objective and supported by the cited sources. Note that the optimal dosage of polypropylene fibre for concrete is not ‘the more the better’. Excessive amounts of polypropylene fibre can reduce the mechanical properties of concrete and its frost resistance. The optimal dose should be carefully determined [12,14,15,20].

The rapid development of artificial intelligence technology in recent years has made the concrete field more and more intelligent. Compared with the traditional concrete design tests in which a lot of time and cost are required to obtain targeted results, the prediction of concrete mechanical properties and other characteristics using artificial neural networks can save a lot of time and cost, so it is equally important to accurately predict the strength changes of concrete under the influence of nonlinear characteristics and external multifactors. It has been shown that the effectiveness of model prediction depends on a finite number of parameters, including the quality and quantity of the data set, the model type, and the input and output correlations [21]. When investigating predictive models for the mechanical properties of concrete, most scholars have used the traditional backpropagation neural network algorithm (BPNN) for the prediction of concrete strength. However, these initial neural network solution processes can easily fall into the trap of local optimal solutions. In addition, the computational power and speed of these embedded algorithms may not be sufficient when dealing with complex functions as objectives.

To avoid local minima while speeding up computation, algorithm fusion can be used to improve the performance of optimisation algorithms. Recent studies have shown that

the use of intelligent algorithms to optimise the parameters of neural network models can improve their generalisation ability to predict the mechanical properties of conventional concrete. Certain intelligent optimisation algorithms have been introduced by some scholars to improve the shortcomings of backpropagation neural networks, including, but not limited to, Genetic Algorithms (GA), Particle Swarm Optimization (PSO), the Sparrow Search Algorithm (SSA), and Random Forest Algorithms (RF). The number of hidden layers and the optimal number of neurons in each hidden layer significantly affect BPNN performance. To determine these two values, traditional trial and error methods are widely used, wasting effort and time. These intelligent optimisation algorithms test the number of hidden layers and the optimal number of neurons by their own logic and optimise and improve the weights and thresholds of the BPNN, which improves the convergence speed of the BPNN, prevents the neural network from falling into a local optimum, and improves the prediction accuracy of the BPNN and the reliability of the results [22–24]. The Beetle Antenna Search (BAS) was proposed in 2017 as an intelligent optimisation algorithm similar to the Particle Swarm Algorithm and Genetic Algorithm. Compared with algorithms such as PSO and GA, BAS utilises an adaptive step-size mechanism to achieve balanced exploration and development and does not require knowledge of the specific form of the function or gradient information, which greatly reduces the amount of computation and effectively achieves the optimal search for the number of hidden layers and the optimal number of neurons. Meanwhile, BAS is particularly effective for improving the weights and thresholds of the BPNN during the optimisation training process, which improves the convergence speed and computational power of the BPNN while preventing the BPNN from falling into local optimums, and improves the reliability and accuracy of the prediction of the BPNN [25–36].

This paper focuses on the Northwest Jingdian Irrigation District as the research area. Clear water, 3% NaCl, and 5% Na₂SO₄ were selected as the main freezing and thawing mediums to simulate the actual environment of the concrete building in the project. The salt-freezing performance of fibre concrete was tested using the fast-freezing method. The objective of this study is to clarify the freezing process of fibre concrete in different freezing and thawing media with varying dosages. Additionally, the study aims to reveal the damage mechanism and investigate the effect of different dosages of polypropylene fibres on the mechanical properties of fibre concrete after salt freezing. Meanwhile, while the experimental method is an effective way to study the performance of PPFRC, it can be time consuming and resource intensive. Therefore, to ensure its safe use in structures, it is of great practical significance to predict the compressive strength of concrete more accurately. This can be achieved by constructing a strength prediction model that combines intelligent algorithms and artificial neural networks. Such a model can more accurately predict changes in concrete strength in the presence of nonlinear characteristics and the influence of multiple external factors. By combining intelligent algorithms and artificial neural networks, a strength prediction model can accurately predict the change in the strength of concrete under the influence of nonlinear characteristics and external factors. This solves the problem of time-consuming and costly laboratory testing for mix and ratio design.

2. Materials and Methods

2.1. Test Material and Proportion Design

For the test, we selected Zhengzhou Tianrui P.O42.5 cement, and its technical specifications are presented in Table 1 (data from the manufacturer). The coarse aggregate used consisted of 5–20 mm continuously graded stones from the Zhengzhou sand and gravel quarry, with a ratio of 3:2 between large and small stones. The natural river sand from Nanyang City was selected as the fine aggregate for this study. The sand used in this test has a grain size in the range of 0.25 mm–0.5 mm, belongs to medium sand in Zone II, and its parameters are shown in Table 2 (data from the manufacturer). The polypropylene fibre used in this study was produced by Shuangyuan Energy Conservation Science and

Technology Co. Table 3 displays the characteristics of polypropylene fibre manufactured by Shuangyuan Energy Saving Technology Co., Ltd (Langfang, Hebei Province, China). To enhance the freezing resistance of the concrete matrix, air reducing agent, water-entraining agent, and fly ash were added during specimen preparation. Table 4 provides specific details on the materials used.

Table 1. P.O42.5 Cement strength index MPa.

Projects	3d Compressive Strength	28d Compressive Strength	3d Flexural Strength	28d Flexural Strength
Standard value	≥17.0	≥42.5	≥3.5	≥6.5
Measured value	26.5	45.9	5.8	8.1

Table 2. Sand performance index.

Fineness Module	Apparent Density/kg/m ³	Packing Density/kg/m ³	Water Absorption/%	Mud Content/%
2.74	2589	1430	1.3	1.8

Table 3. Polypropylene fibre performance table.

Material Name	Fibre Length/mm	Monofilament Diameter/μm	Densities/g/cm ³	Modulus of Elasticity/GPa	Tensile/MPa	Melting Point/°C
PPF	19	12	0.91	7.2	745	166

Table 4. Mix design table.

Number (PPF)	Fibre Content kg/m ³	Water-to-Cement Ratio	Cement kg/m ³	Water kg/m ³	Fine Aggregate kg/m ³	Coarse Aggregate kg/m ³	Coal Ash kg/m ³	Air-Entraining Agent g/m ³	Water-Reducing Agent kg/m ³
PC	0	0.45	272	175	642	1193	117	19.45	3.8
PPF0.3	0.3	0.45	272	175	642	1193	117	19.45	3.8
PPF0.6	0.6	0.45	272	175	642	1193	117	19.45	3.8
PPF0.9	0.9	0.45	272	175	642	1193	117	19.45	3.8
PPF1.2	1.2	0.45	272	175	642	1193	117	19.45	3.8

2.2. Freeze–Thaw Test Design

In accordance with GB/T 50082-2009 ‘Long-term Performance and Durability Test Method of Ordinary Concrete’, the freeze–thaw cycle test is conducted using the ‘fast freezing method’. See Figure 1 for basic principles. After 24 days of curing, the PPFRC is removed and immersed in 3 different solutions for 4 days. Following this, the PPFRC is placed in the test box of the freezing and thawing machine equipped with the corresponding freezing and thawing medium and the freezing and thawing process is initiated. The time for one freeze–thaw cycle should be set at approximately 4 h. Additionally, the melting time of the PPFRC should account for more than one-quarter of the total time. Simultaneously, the specimen’s centre temperature must range from −20 °C to 7 °C, and its warming and cooling process should comprise more than half of the total thawing or freezing time. Following the test design, the mechanical properties of the PPFRC were measured every 25 times and subsequently placed in the test box with the corresponding salt solution for further testing. The stopping test shall meet the following criteria: (1) 300 cycles; (2) the dynamic elasticity model is reduced to 60% of the original; (3) the loss of mass is more than 5% of the original mass. In this test, 150 freeze–thaw cycles were carried out to meet the criteria for stopping the test.

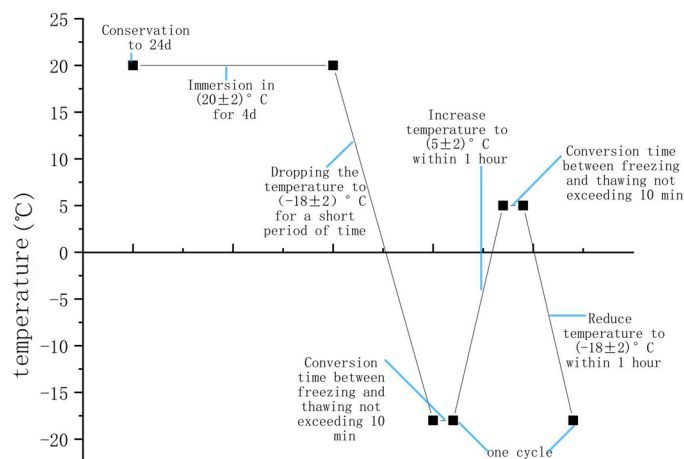


Figure 1. Temperature–time diagram of the “fast-freezing method”.

2.3. Test Results

2.3.1. Changing Law of PPFRC Mass Loss under Three Freeze–Thaw Conditions

The Tables 5–7 and Figure 2 show shows that the mass loss of each group is slow in the early stage and rapid in the late stage of freezing and thawing in water and 3% NaCl medium. In 5% Na₂SO₄ freezing and thawing medium, there is a small increase in mass in the early stage and rapid growth in the late stage. The effect of different freezing and thawing environmental factors on concrete mass loss is smallest in clear water solution and largest in 3% NaCl solution. The effect of PPF doping on matrix mass loss improvement is as follows: PPF1.2 > PPF0.9 > PPF1.5 > PPF0.6 > PC. The degree of improvement in matrix quality loss follows the same order.

Table 5. PPFRC mass loss rate under clear water freeze–thaw conditions (%).

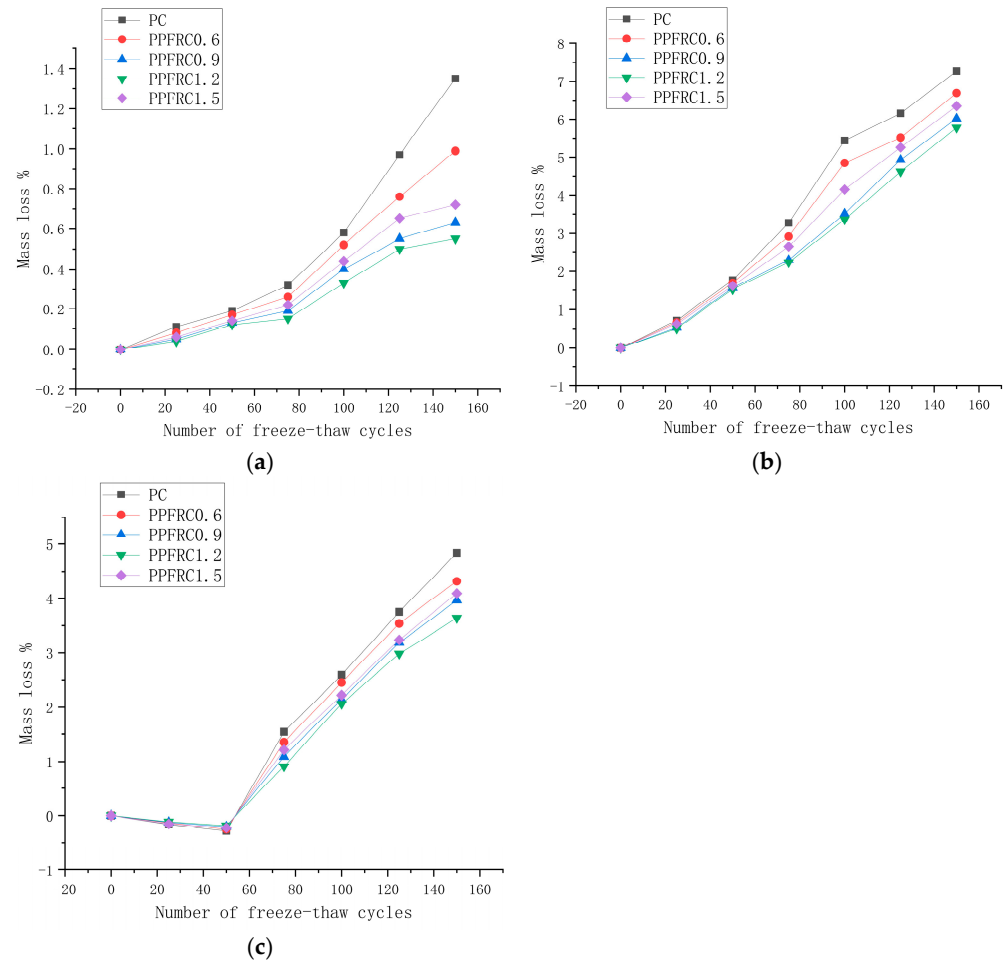
Number of Freeze–Thaw Cycles	PC	PPFRC0.6	PPFRC0.9	PPFRC1.2	PPFRC1.5
0	0.00	0.00	0.00	0.00	0.00
25	0.11	0.08	0.05	0.04	0.06
50	0.19	0.17	0.13	0.12	0.14
75	0.32	0.26	0.19	0.15	0.22
100	0.58	0.52	0.4	0.33	0.44
125	0.97	0.76	0.55	0.5	0.65
150	1.35	0.99	0.63	0.55	0.72

Table 6. PPFRC mass loss rate under 3% NaCl freeze–thaw conditions (%).

Number of Freeze–Thaw Cycles	PC	PPFRC0.6	PPFRC0.9	PPFRC1.2	PPFRC1.5
0	0.00	0.00	0.00	0.00	0.00
25	0.72	0.67	0.54	0.51	0.63
50	1.76	1.69	1.56	1.52	1.61
75	3.27	2.92	2.29	2.23	2.64
100	5.44	4.85	3.51	3.36	4.15
125	6.16	5.52	4.93	4.62	5.26
150	7.27	6.69	6.02	5.78	6.35

Table 7. PPFRC mass loss rate under 5% Na₂SO₄ freeze–thaw conditions (%).

Number of Freeze–Thaw Cycles	PC	PPFRC0.6	PPFRC0.9	PPFRC1.2	PPFRC1.5
0	0.00	0.00	0.00	0.00	0.00
25	−0.16	−0.13	−0.12	−0.11	−0.15
50	−0.28	−0.25	−0.2	−0.18	−0.22
75	1.54	1.35	1.09	0.91	1.21
100	2.59	2.45	2.14	2.06	2.22
125	3.75	3.54	3.19	2.98	3.24
150	4.84	4.32	3.96	3.64	4.09

**Figure 2.** Quality loss rate. (a) Clear water; (b) 3% NaCl; (c) 5% Na₂SO₄.

2.3.2. Relative Dynamic Elastic Modulus Degradation Patterns of PPFRC under Three Freeze–Thaw Conditions

Referring to GB/T 50082-2009, the dynamic elastic modulus of concrete was determined by the resonance method. The measuring instrument makes the specimen produce forced vibration, with the help of the wave propagating in the concrete, under the condition that Poisson's ratio, density and length of the material are unchanged, the wave speed (fundamental frequency = wave speed/length of the material) and the elastic modulus of the material are in accordance with a certain functional relationship. Thus, the fundamental frequency of the material is measured by the resonance method, and the modulus of elasticity of the material can be deduced, which is called the dynamic modulus of elasticity to distinguish it from the conventional modulus of elasticity.

The Table 8 and Figure 3 show that the dynamic elastic modulus of each group decreased gradually with an increase in the number of freezing and thawing cycles. After

50 cycles, the rate of decrease accelerated, and the decrease was different for each group. At 150 cycles, the relative modulus of kinetic elasticity for PC, PPFRC0.6, PPFRC0.9, PPFRC1.2, and PPFRC1.5 were 66.34%, 72.87%, 78.31%, 80.68%, and 75.49%, respectively, which did not drop below 60%. The relative modulus of kinetic elasticity of PPF-mixed concrete is significantly higher than that of ordinary concrete. The best performance is observed in the PPFRC1.2 group. In clear water, the relative modulus of kinetic elasticity of concrete groups under the same number of freeze–thaw cycles follows the following order: PPFRC1.2 > PPFRC0.9 > PPFRC1.5 > PPFRC0.6 > PC.

Table 8. PPFRC relative dynamic elastic modulus under clear water freeze–thaw (%).

Number of Freeze–Thaw Cycles	PC	PPFRC0.6	PPFRC0.9	PPFRC1.2	PPFRC1.5
0	100	100	100	100	100
25	99.62	99.71	99.74	99.77	99.73
50	99.26	99.38	99.52	99.55	99.49
75	93.58	94.83	95.62	96.28	95.41
100	83.35	86.32	88.47	90.24	87.47
125	76.26	78.87	83.75	85.44	81.66
150	66.34	72.87	78.31	80.68	75.49

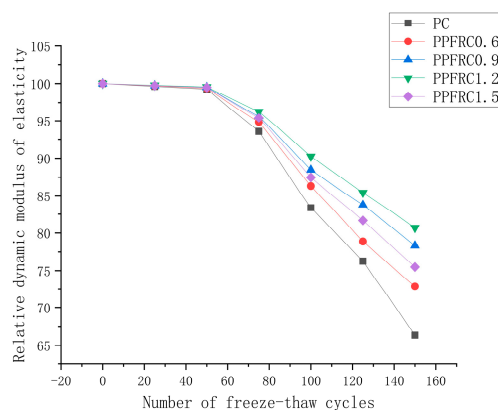
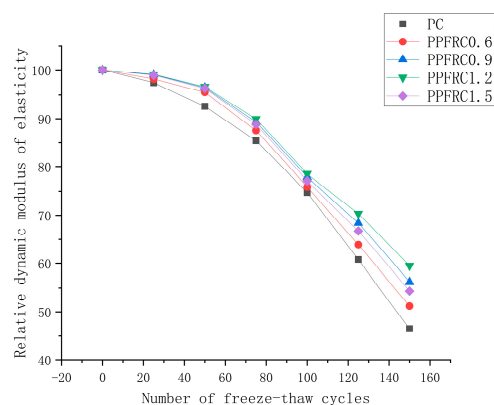


Figure 3. Relative dynamic modulus of elasticity of clear water.

The Table 9 and Figure 4 show that, in the freezing and thawing medium containing 3% NaCl, the relative dynamic elastic modulus decreased significantly at the early stage. As the number of freezing and thawing cycles accumulated, the relative dynamic elastic modulus decreased slowly at first and then rapidly. After undergoing 150 cycles of freezing and thawing, the relative dynamic elastic modulus of P C, PPFRC0.6, PPFRC0.9, PPFRC1.2, PPFRC1.5 were 46.50%, 51.24%, 56.23%, 59.49%, 54.37%, respectively. It is worth noting that the relative dynamic elasticity modulus of all the groups was lower than 60%, indicating that the mechanical properties of all the groups were severely damaged after 150 cycles of salt-freezing. Therefore, it can be concluded that the mechanical properties of each group were significantly affected after undergoing 150 cycles of salt-freezing. In the freezing and thawing medium of 3% NaCl, the relative dynamic elastic modulus of the concrete groups, under the same number of freezing and thawing cycles, followed this order: PPFRC1.2 > PPFRC0.9 > PPFRC1.5 > PPFRC0.6 > PC.

Table 9. PPFRC relative dynamic elastic modulus under 3% NaCl freeze–thaw (%).

Number of Freeze–Thaw Cycles	PC	PPFRC0.6	PPFRC0.9	PPFRC1.2	PPFRC1.5
0	100	100	100	100	100
25	97.48	98.2	99.06	99.11	98.95
50	92.61	95.54	96.48	96.65	96.34
75	85.42	87.54	89.34	89.98	88.83
100	74.75	75.91	77.92	78.56	77.15
125	60.79	63.87	68.39	70.36	66.72
150	46.5	51.24	56.23	59.49	54.37

**Figure 4.** Relative dynamic modulus of elasticity of 3% NaCl.

The Table 10 and Figure 5 show that, in the freezing and thawing medium of 5% Na_2SO_4 , the decrease was slow before 50 cycles of freezing and thawing. After 50 cycles but before 100 cycles, the decrease in each group reached its maximum. The PC group experienced the largest decrease, while the decrease of PPFRC1 was also significant. After 100 cycles, the rate of decrease in each group gradually slowed down. The relative kinetic elastic modulus of PC, PPFRC0.6, and PPFRC1.5 was lower than 60%, indicating serious damage after 125 cycles of freezing and thawing. The values were 53.27%, 57.12%, and 59.35%, respectively. After undergoing 125 cycles of freezing and thawing, PC, PPFRC0.6 and PPFRC1.5 exhibited a relative dynamic elastic modulus lower than 60%, indicating serious damage. Specifically, the values were 53.27%, 57.12%, and 59.35%, respectively. On the other hand, the relative dynamic elastic modulus of PPFRC0.9 and PPFRC1.2 were 62.34% and 66.94%, respectively, which did not meet the criteria for serious damage. In a 5% Na_2SO_4 freezing and thawing medium, the relative dynamic elastic modulus of concrete groups under the same number of freezing and thawing times follows this order: PPFRC1.2 > PPFRC0.9 > PPFRC1.5 > PPFRC0.6 > PC.

Table 10. PPFRC relative dynamic elastic modulus under 5% Na_2SO_4 freeze–thaw (%).

Number of Freeze–Thaw Cycles	PC	PPFRC0.6	PPFRC0.9	PPFRC1.2	PPFRC1.5
0	100	100	100	100	100
25	98.35	99.48	99.6	99.64	99.56
50	97.51	98.25	98.68	98.97	98.45
75	89.76	90.25	92.84	93.23	91.85
100	76.46	78.42	81.49	83.16	80.77
125	64.35	66.16	74.57	77.46	71.74
150	53.27	57.12	62.34	66.94	59.35

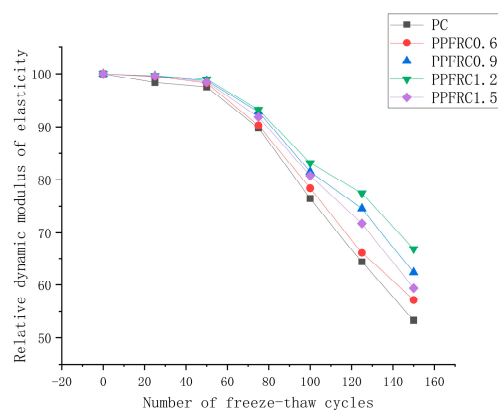


Figure 5. Relative dynamic modulus of elasticity of 5% Na₂SO₄.

Based on the charts provided, the relative dynamic elastic modulus of each group decreases as the number of freeze–thaw cycles increases under three different conditions. The decline is generally slow at first, followed by a sharp decrease. Before undergoing 50 cycles of freezing and thawing, the rate of decrease in weight of each specimen in water and 5% Na₂SO₄ solution was similar, with a slow decrease. However, in 3% NaCl solution, the decrease was more pronounced. After 50 cycles of freezing and thawing, the rate of decrease in weight of each specimen in all 3 solutions rapidly accelerated. Upon reaching 150 cycles of freezing and thawing, the PC group exhibited the worst overall performance, with the relative dynamic elastic modulus being the lowest in all 3 media. The optimal group for the overall performance of PPFRC1.2 has relative dynamic elastic modulus values of 80.68%, 59.49%, and 66.94% in the 3 media, respectively. The results demonstrate that the ordinary concrete and the PPF-added concrete have similar properties. Both ordinary concrete and concrete with PPF exhibited the least freeze–thaw damage in water and the most freeze–thaw damage in a 3% NaCl solution. The relative dynamic elastic modulus of the specimens decreases due to the internal pores and cracks increasing under the action of salt-freezing coupling. This is one of the main reasons for the decrease. Chlorine salts, sulphates, and cement mortar react with each other to generate crystallisation. The increase in the number of crystals results in concrete having a crystallisation pressure and expansion pressure, which also leads to an increase in the number of internal pores and cracks. Compared to regular concrete, the addition of an appropriate amount of PPF can significantly enhance the relative dynamic elastic modulus of concrete when exposed to salt-freezing erosion. It can also reduce the extent of salt freezing damage to concrete to some degree. In summary, the relative dynamic elastic modulus undergoes the greatest change in a 3% NaCl solution under different freezing and thawing environments, followed by a 5% Na₂SO₄ solution. The degree of improvement of the dynamic elastic modulus of the matrix after freezing with different PPF dosages is in the following order: PPF1.2 > PPF0.9 > PPF1.5 > PPF0.6 > PC.

2.3.3. Deterioration Pattern of Compressive Strength of PPFRC under Three Freeze–Thaw Conditions

Table 11 shows that the addition of PPF to PC can significantly enhance its matrix strength. At a fibre dosage of 0.6 kg/m³, the effect on concrete strength is not significant. However, at a dosage of 1.2 kg/m³, the strength of concrete is optimised, resulting in a 16.14% increase in strength and a compressive strength increase of 7.15 MPa. At a dosage of 1.5 kg/m³, the rate of increase in compressive strength is lower, but the baseline strength is still higher than that of the compressive strength of the PC and PPFRC0.6 group. At a dosage of 1.5 kg/m³, the rate of increase in compressive strength of the concrete decreased. However, the baseline strength remained higher than that of the PC and PPFRC0.6 groups. It can be concluded that the average compressive strength of plain concrete can be increased

to a certain extent by adding an appropriate amount of PPF. However, excessive amounts will lead to a decrease in concrete strength.

Table 11. Effect of PP dosing on initial concrete strength.

Number	Doping Level/(kg/m ³)	Average Compressive Strength/(MPa)	Strength Increase/%
PC	0	44.37	0
PPFRC0.6	0.6	46.43	4.64
PPFRC0.9	0.9	48.26	8.77
PPFRC1.2	1.2	51.52	16.14
PPFRC1.5	1.5	47.71	7.53

The Table 12 and Figure 6 show that the compressive strengths of the four PPFRC groups in clear water freezing and thawing media increased at different rates compared to the PC group. Additionally, the compressive strengths showed a slower rate of decrease initially, followed by a faster rate of decrease as the number of freezing and thawing times accumulated. Prior to undergoing 75 cycles of freezing and thawing, the PPFRC1.2 group exhibited the slowest decrease in compressive strength. Subsequently, the compressive strength of each group decreased at an accelerated rate. The PC group displayed the largest decrease, while the PPFRC1.2 group exhibited the smallest decrease. The PPFRC1.5 group demonstrated lower strength compared to the PPFRC0.9 group. The decreasing trends were similar across all groups. In the medium of freshwater freezing and thawing, the compressive strengths of the concrete groups, under the same number of freezing and thawing cycles, follow this order: PPFRC1.2 > PPFRC0.9 > PPFRC1.5 > PPFRC0.6 > PC.

Table 12. PPFRC compressive strength under clear water freeze–thaw conditions (MPa).

Number	PC	PPFRC0.6	PPFRC0.9	PPFRC1.2	PPFRC1.5
0	44.35	46.44	48.7	51.83	47.69
25	43.61	45.82	48.53	51.75	47.32
50	42.54	45.05	47.98	51.32	46.66
75	40.71	43.67	47.03	50.54	45.55
100	37.92	40.61	44.87	48.61	43.46
125	34.18	37.16	41.97	45.29	41.23
150	30.66	33.85	37.72	40.67	36.51

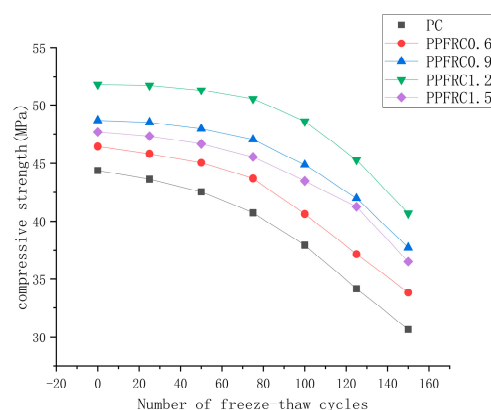


Figure 6. Compressive strength of the test samples in a clean water environment.

The Table 13 and Figure 7 show that, in the freezing and thawing medium containing 3% NaCl, each group exhibited a more pronounced decreasing trend in the early stage. Before undergoing 50 cycles of freezing and thawing, the PC group and PPFRC0.6 group exhibited a faster decrease in compressive strength. PPFRC0.9, PPFRC1.2, and PPFRC1.5

exhibited a slower decrease, with a similar decreasing trend. After 50 cycles of freezing and thawing, the compressive strength of each group gradually decreased at a faster rate. The PC group exhibited the largest decrease, followed by PPFRC0. The decreasing rate of PC was the smallest, while that of PPFRC1.2 was the largest. At 150 cycles of freezing and thawing, the compressive strength of PC, PPFRC0.6, PPFRC0.9, PPFRC1.2, and PPFRC1.5 decreased to 48.91%, 58.13%, 65.56%, 66.44%, and 62.12% of their initial strength, respectively. The salt-freezing and thawing damages in the specimens of PC and PPFRC0.6 groups were severe, with obvious aggregate bare. The salt freeze–thaw damage was severe in the PC and PPFRC0.6 groups, resulting in significant aggregate exposure and slagging. In contrast, the damage was less severe in the remaining three groups. The compressive strengths of the concrete groups with the same number of freezing and thawing times in the 3% NaCl freezing and thawing medium were as follows: PPFRC1.2 > PPFRC0.9 > PPFRC1.5 > PPFRC0.6 > PC

Table 13. PPFRC compressive strength under 3% NaCl freeze–thaw conditions (MPa).

Number	PC	PPFRC0.6	PPFRC0.9	PPFRC1.2	PPFRC1.5
0	44.31	46.43	47.98	51.13	47.6
25	43.37	45.64	47.39	50.59	46.93
50	40.53	43.02	45.88	49.33	45.19
75	35.69	38.81	42.18	45.95	41.31
100	30.15	33.67	37.86	41.34	36.41
125	25.51	30.22	34.49	37.96	32.55
150	21.67	26.99	31.39	33.91	29.57

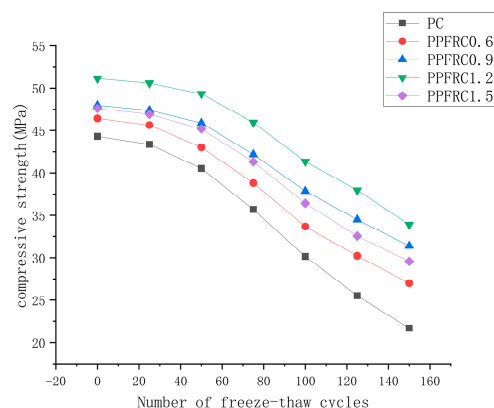


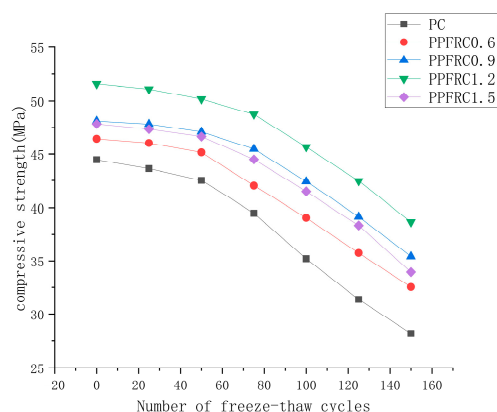
Figure 7. Compressive strength of the test sample in a 3% NaCl solution environment.

The Table 14 and Figure 8 show that, In the freeze–thaw medium of 5% Na₂SO₄, the groups exhibited a slow decrease in their phase compressive strength in the early stage. However, with an increasing number of freeze–thaw cycles, the decrease rate showed a slow-to-rapid situation. After 150 cycles of freezing and thawing, the compressive strengths of PC, PPFRC0.6, PPFRC0.9, PPFRC1.2, and PPFRC1.5 were reduced to 63.33%, 70.06%, 73.66%, 74.92%, and 70.96% of their initial strengths, respectively. The order of magnitude of compressive strength exhibited by concrete specimens mixed with different contents of polypropylene fibres in 5% sodium sulphate freezing and thawing medium at the same number of freeze–thaw cycles is as follows:

$$\text{PPFRC1.2} > \text{PPFRC0.9} > \text{PPFRC1.5} > \text{PPFRC0.6} > \text{PC}.$$

Table 14. PPFRC compressive strength under 5% Na₂SO₄ freeze–thaw conditions (MPa).

Number	PC	PPFRC0.6	PPFRC0.9	PPFRC1.2	PPFRC1.5
0	44.45	46.43	48.1	51.6	47.83
25	43.62	46.03	47.81	51.12	47.35
50	42.51	45.15	47.08	50.18	46.65
75	39.48	42.02	45.48	48.74	44.49
100	35.21	39.06	42.41	45.66	41.47
125	31.36	35.75	39.16	42.46	38.35
150	28.15	32.53	35.43	38.66	33.94

**Figure 8.** Compressive strength of the test sample in a 5% Na₂SO₄ solution environment.

Some studies have shown that when fibre is added to concrete, fibre can easily, quickly and evenly disperse in concrete to produce a restraining effect on concrete. At the same time, fibre itself has a certain strength, which can disperse the stress of part of concrete, prevent the occurrence and development of primary cracks in concrete, and improve the crack resistance of concrete to improve its mechanical properties and freeze–thaw resistance, thus extending the service life of the concrete.

In this test, the mechanical properties and frost resistance of polypropylene fibre concrete with a fibre yield of 1.2 kg/m³ are the best. The possible reason is that when the fibre content is less than 1.2 kg/m³, the constraint of polypropylene fibre on the cement slurry is small, resulting in the limited improvement of the compressive capacity of the sample; while when the fibre content is greater than 1.2 kg/m³, too many fibres will agglomerate, resulting in the increase of the weak interface of the concrete, and the damage may first occur in the freeze–thaw process. When the damage effect of the weak interface is greater than the reinforcement effect of the fibre, the mechanical properties of the concrete are reduced. The content of 1.2 kg/m³ polypropylene fibre makes the fibre in the maximum constraint of the cement slurry at the same time as possible not to agglomerate, thus enhancing the mechanical properties of concrete and frost resistance.

3. PPFRC Strength Prediction Model

3.1. Predictive Modelling Fundamentals

(1) Principle of the BPNN model

A BPNN is a neural network structure that uses the backpropagation algorithm. When the input data reaches the output layer, the network calculates the root mean square error between the predicted value and the input value. If this error is greater than the set value, it is transmitted in the reverse direction. During this process, the weighted value and threshold are gradually adjusted until the error reaches the design value, at which point the network stops running. The test's BPNN model utilises a network structure with a single hidden layer. It takes five input values: fibre volume doping, volume fraction of three types of freeze–thaw medium doping, and the number of freeze–thaw times. The

output value is the compressive strength. The number of neurons in the hidden layer is determined by the Formula (1) to establish the range.

$$N_h = \frac{N_s}{(a * (N_i + N_o))} \tag{1}$$

where: N_h is the number of neurons; N_s is the number of training samples; N_i and N_o are the number of input and output layers, respectively; 'a' is a self-taken arbitrary value ranging from 2 to 10; the number of neurons in the hidden layer ranges from 1 to 9, and the number of neurons is preferred through several trials and combined with the evaluation index, and the preferred number of neurons is determined to be 8, therefore, the BPNN model is used in the present study. The basic principle and composition of the BPNN model in this study are shown in Figure 9.

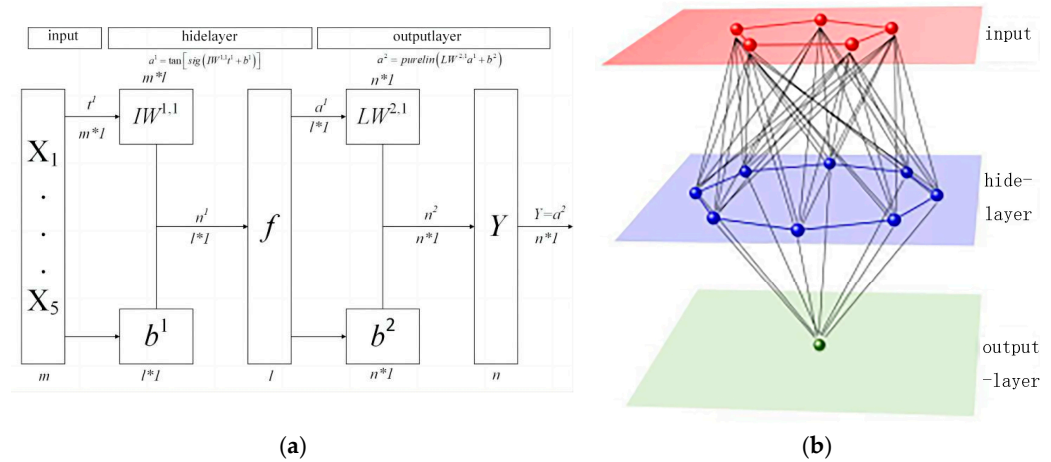


Figure 9. Principle of BPNN prediction model and network architecture. (a) Flowchart of a neural network transmitting information; (b) Structure of the neural network model.

(2) Principle of BAS

The BAS algorithm is a recent proposal for optimizing multi-objective functions. It has the advantages of small computational requirements, fast convergence, and global optimality search. The formula for updating the spatial coordinates and position of tensors is provided below.

$$x_l = x + d_0 * \frac{\vec{b}}{2} f(x_l) < f(x_r) \tag{2}$$

$$x_r = x - d_0 * \frac{\vec{b}}{2} f(x_l) > f(x_r) \tag{3}$$

$$x^{t+1} = x^t - \delta^t * \vec{b} * \text{sign}(f(x_{rt}) - f(x_{lt})) \tag{4}$$

where: x is the coordinates of the centre of mass; x_l is the coordinates of the left whisker; x_r is the coordinates of the right whisker; d_0 is the difference between the distances of the left and right whiskers; x^t, x^{t+1} are the coordinates of the centre of mass in the t th and $t + 1$ st iteration; δ^t is the value of the step factor after t times of turnover; $\text{sign}()$ is the sign function.

3.2. Establishment of BAS-BP Model and Evaluation Indicators

The stand-alone backpropagation neural network (BPNN) is limited by the initial set values of the parameters and is prone to local optimization rather than global optimization. To improve the global optimization capability of the BPNN, the Bat Algorithm (BAS) is introduced. The weights and biases of the BPNN model are randomly initialized, and then the weights and thresholds are introduced as the initial positions of the BAS. When

the termination condition is satisfied, an optimal position is obtained for the BAS. The initial weights and thresholds are reformatted to achieve the optimal position. The BPNN model is then trained using the classical optimization algorithm, which has been debugged beforehand. Finally, the BAS-BP prediction model is constructed.

A model was created to forecast the compressive strength of PPFRC under varying numbers of freeze–thaw cycles. The model’s performance was quantitatively evaluated using four statistical parameters: root mean square error (*RMSE*), the dispersion index (*SI*), mean absolute percentage error (*MAPE*), and coefficient of determination (R^2).

$$RMSE = \sqrt{\frac{1}{N} \sum_{t=1}^N (observed_t - predicted_t)^2} \quad (5)$$

$$SI = RMSE / \overline{observed_t} \quad (6)$$

$$MAPE = \sum_{t=1}^N \left| \frac{observed_t - predicted_t}{observed_t} \right| * \frac{100\%}{N} \quad (7)$$

$$R^2 = 1 - \left(\frac{\sum_{t=1}^N (observed_t - predicted_t)^2}{\sum_{t=1}^N predicted_t^2} \right) \quad (8)$$

The model’s performance can be classified into four levels based on the *SI* value, where *N* is the number of samples, *observed* is the actual value, and *predicted* is the predicted value. These levels are excellent ($SI < 0.1$), good ($0.1 < SI < 0.2$), fair ($0.2 < SI < 0.3$), and poor ($SI > 0.3$). Models with high performance have *RMSE*, *SI*, and *MAPE* values close to 0, and an R^2 value close to 1.

In order to provide a comprehensive assessment of the predictive performance of the proposed model, a composite performance metric is used as shown in the following equation:

$$precision = \left(\frac{n_{tr} RMSE_{tr} + SI_{tr} + MAPE_{tr}}{n_{all} R_{tr}^2} \right) + \left(\frac{n_{tst} RMSE_{tst} + SI_{tst} + MAPE_{tst}}{n_{all} R_{tst}^2} \right) \quad (9)$$

where the subscripts *tr*, *tst*, and *all* represent model training, testing and all data, respectively.

Based on this, all models can be ranked from worst to best according to the precision value. Obviously, the model with better overall performance should have the lowest precision value. Meanwhile, in order to verify whether the BAS-BP prediction model is better than other intelligent algorithm models used for predicting concrete strength, the Genetic Algorithm (GA) and Particle Swarm Algorithm (PSO) are added to optimise the prediction model of the BPNN, and, finally, the prediction accuracy is compared with the BAS-BP model.

4. Evaluation of Prediction Model Accuracy

Table 15 displays the performance metrics of the four developed models. As all R^2 values are greater than 0.900, the models demonstrate strong agreement with the actual results. The table shows that the BPNN prediction models improved by the BAS and PSO algorithms had a better fit, while the GA-BP model showed little improvement. The BAS-BP model had the fastest convergence rate, leading to the conclusion that it is the most effective overall. This suggests that the model can be applied to predict the strength of the PPFRC under salt freezing. Figure 10 displays the prediction results of the BAS-BP test set and its adaptation curve, respectively. The three optimised BPNN models exhibit superior performance compared to the conventional BPNN model. This suggests that enhancing the initial weights and biases in the intelligent algorithm can enhance the performance of the BPNN models. The *SI* values of all models are below 0.1, with BAS-BP having the lowest *SI* value. All three improved BPNN models demonstrate superior performance compared

to the independent BPNN model. This further confirms the effectiveness of the swarm intelligence algorithm in enhancing the prediction accuracy of the BPNN model.

Table 15. Comparison of performance indicators of all prediction models.

Performance Index	Dataset	BPNN	BAS-BP	GA-BP	PSO-BP
RMSE	Training	1.3074	0.8778	1.0029	0.9954
	Testing	2.0202	1.2091	1.8707	1.6799
	All	1.5596	0.9906	1.3288	1.2445
SI	Training	0.0310	0.0212	0.0241	0.0246
	Testing	0.0489	0.0287	0.0440	0.0395
	All	0.0372	0.0236	0.0317	0.0297
MAPE	Training	0.0234	0.0153	0.0188	0.0167
	Testing	0.0411	0.0271	0.0375	0.0346
	All	0.0288	0.0189	0.0245	0.0222
R^2	Training	0.9601	0.9812	0.9798	0.9749
	Testing	0.9204	0.9741	0.9356	0.9571
	All	0.9460	0.9782	0.9645	0.9676
CPU-time/s		2	28	83	45

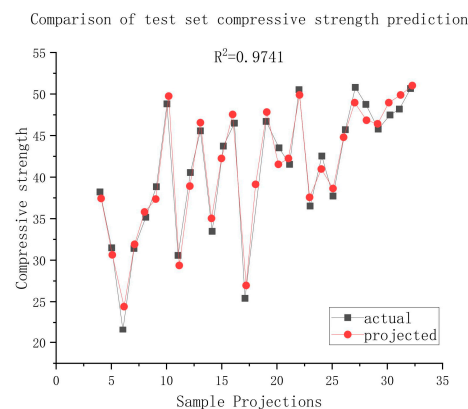


Figure 10. The prediction results of the BAS-BP test set.

In order to further confirm the performance of the proposed BAS-BP models, Figure 11 shows the fitting relationships between the experimental and predicted results of all models. According to the fitting results and the distribution of confidence intervals, the BAS-BP model has smaller residual variations and the confidence intervals tend to be more similar to the fitted line than the other models, which indicates that the BAS algorithm can effectively improve the prediction accuracy, and the prediction performance of the selected models can be ranked as BAS-BP > PSO-BP > GA-BP > BPNN.

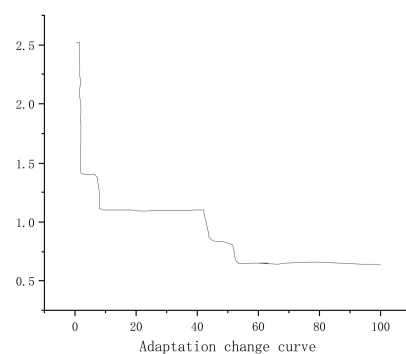


Figure 11. BAS-BP fitness function change curve.

Figure 12 and Table 16 show the precision values for the four developed models. Among all the models, the standalone BPNN model has the worst overall performance and the largest precision value, while the BAS-BP model shows the best overall performance, with the precision values of BAS-BP, GA-BP, and PSO-BP being 47.12%, 6.4%, and 23.01% lower than those of the standalone BPNN model, which is consistent with the conclusions of the SI-based analyses. This is consistent with the conclusion of the SI-based analysis.

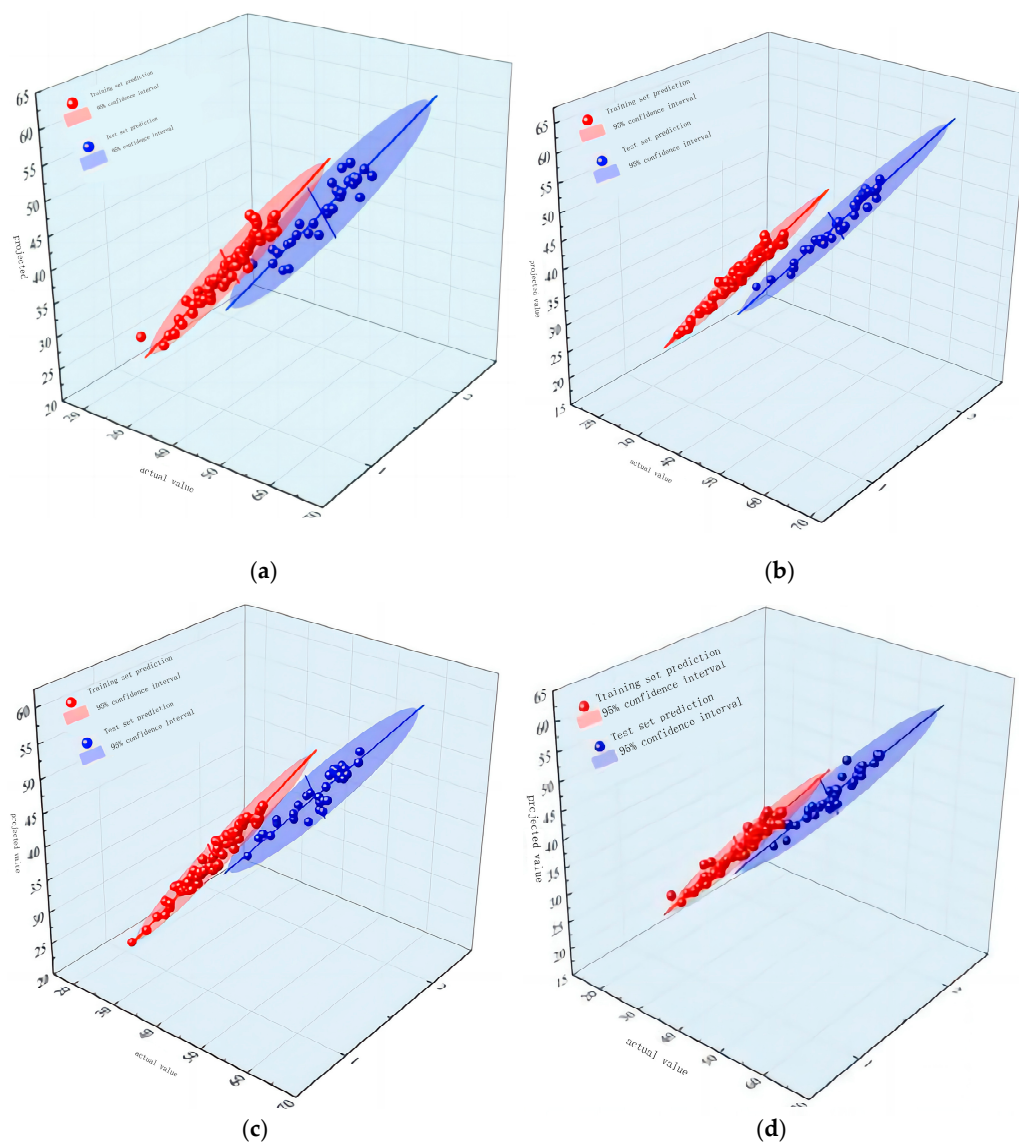


Figure 12. Fitting the prediction results of the training set and test set of the four prediction models. (a) BPNN; (b) BAS-BPNN; (c) GA-BPNN; (d) PSO-BPNN.

Table 16. Precision value of the development model.

Models	BPNN	BAS-BP	GA-BP	PSO-BP
Precision	1.7863	1.0665	1.4371	1.3419

In conclusion, this study demonstrates that the implementation of intelligent algorithms to optimize the parameters of the artificial neural network model can enhance its generalization ability in predicting the mechanical properties of concrete. This approach effectively addresses the issues of complexity, non-linearity, and modelling difficulties en-

countered in the freezing process of concrete. Furthermore, it provides relatively accurate predictions at a lower cost than traditional experimental methods.

5. Conclusions

1. When the freezing and thawing medium and the number of cycles are the same, all four groups of PFRC perform better than the PC control group in all four evaluation indices. This suggests that polypropylene fibre can improve the mechanical properties and freezing resistance of the concrete matrix, delay the process of freezing and thawing damage of the matrix, and increase the life of the matrix, but can not prevent the final failure of the matrix. The conclusions obtained from the summary reasoning of the results of this test are similar to those described in the literature cited in the paper, the appropriate amount of polypropylene fibres can help to enhance the mechanical properties and frost resistance of the concrete specimens, too little fibre content has limited enhancement of the mechanical properties of the specimens, and too much fibre content also reduces the mechanical properties of the specimens. Based on the evaluation indexes of the four groups of PPF-doped specimens, it can be concluded that the PPFRC1.2 group exhibited the best performance. The order of improvement in the macro-physical properties of concrete due to fibre doping is as follows: PPF1.2 > PPF0.9 > PPF1.5 > PPF0.6 > PC.
2. As the number of freezing and thawing cycles increases, the apparent degree of concrete damage and mass loss gradually increase, while the dynamic elastic modulus and compressive strength gradually decrease. It is important to note that the amount of fibre mixing remains constant throughout the process. The relative dynamic elastic modulus and compressive strength of the specimens under different freeze–thaw environments decreased to the extent that 3% NaCl solution environment > 5% Na₂SO₄ solution environment > clear water environment. In the PPFRC1.2 group, following 50 cycles of freezing and thawing in water, a 3% NaCl solution and a 5% Na₂SO₄ solution, the dynamic modulus of elasticity was reduced to 99.55%, 96.65%, and 98.97% of the original, respectively, while the compressive strength was reduced to 99.02%, 96.48%, and 97.25% of the original, respectively. Following 100 cycles of freezing and thawing, the dynamic modulus of elasticity decreased to 90.24%, 78.56%, and 83.16% of its original value, while the compressive strength decreased to 93.79%, 80.85%, and 88.49% of its original value, respectively.
3. Among the prediction models constructed using artificial neural networks, the RMSE and R² values of the BP and BAS-BP models are 1.6405 and 0.9235, and 0.9635 and 0.9733, respectively. The BAS-BP model demonstrates better overall performance in terms of prediction result fitting and performance index comparison. The comparison of overall performance between the BPNN model and the BAS-BP model is further confirmed by the addition of two intelligent algorithms to improve performance. The comparison of overall performance between the BPNN model improved by adding two intelligent algorithms and the BAS-BP model further confirms the superiority and stability of the proposed BAS-BP model. Simultaneously, the proposed BAS-BP model achieves superior performance compared to the traditional BPNN model, enhancing its generalisation ability and applicability. It effectively addresses the issue of the traditional model being prone to local optima and lacking the capacity to handle non-linearities.

Author Contributions: Conceptualization, C.X., J.C. (Jun Cao) and J.C. (Jiaohao Chen); methodology, J.C. (Jun Cao) and J.C. (Jiaohao Chen); software, J.C. (Jun Cao); validation, J.C. (Jun Cao), Z.W., and W.H.; formal analysis, J.C. (Jun Cao); investigation, Z.W.; resources, W.H.; data curation, J.C. (Jun Cao); writing—original draft preparation, J.C. (Jun Cao) and J.C. (Jiaohao Chen); writing—review and editing, J.C. (Jun Cao) and J.C. (Jiaohao Chen); visualization, J.C. (Jun Cao); supervision, C.X.; project administration, C.X.; funding acquisition, N/A. All authors have read and agreed to the published version of the manuscript.

Funding: This research was funded by the Ningxia Water Resources Science and Technology Program (GKGX-KY-2023-001), the Basic Public Welfare Research Program of Zhejiang Province (LZJWD22E090001), and the Major Science and Technology Program of Zhejiang Province (2021C03019).

Data Availability Statement: Data are contained within the article.

Conflicts of Interest: The authors declare no conflicts of interest.

References

1. Xu, C.; Wang, H.; Chen, J.; Li, Z.; Xu, H.; Zi, Y. Influence of Salt Freezing Cycle on Mechanical Properties of Concrete and Its Life Prediction. *J. Water Resour. Power* **2023**, *41*, 134–138. (In Chinese)
2. Xu, C.; Li, Z.; Zhu, X.; Yao, Z.; Wang, M.; Zhuang, P. Study on Mechanical Properties of Concrete Under Sali-Frost-Erosion. *J. Yellow River* **2019**, *41*, 132–136. (In Chinese)
3. Jiang, L.; Niu, D. Study on Damage Failure Criterion of Concrete under Sulfate Attack and Freeze-thaw Environment. *J. Disaster Prev. Mitig. Eng.* **2017**, *37*, 148–153. (In Chinese)
4. Latifi, M.; Biricik, Ö.; Mardani, A. Mechanical and Durability Performance of Macro Polypropylene Fibrous Concrete. *Iran. Polym. J.* **2023**, *32*, 1149–1164. [[CrossRef](#)]
5. Jamenraja, M.C.K.; Ravichandran, K. Structural performance of polypropylene fibre-reinforced concrete beams incorporating nanosilica and alccofine. *Innov. Infrastruct. Solut.* **2023**, *8*, 191. [[CrossRef](#)]
6. Tariq, K.; Ahmad, J.; Husnain, S.; Ijaz, M. Influence on compressive and tensile strength properties of fiber-reinforced concrete using polypropylene, jute, and coir fiber. *J. Mech. Behav. Mater.* **2023**, *32*, 20220263. [[CrossRef](#)]
7. Wang, G.; Yao, P. Experimental Study on Conventional Compressive Strength of Polypropylene Fiber Concrete. *Heilongjiang Hydraul. Sci. Technol.* **2023**, *51*, 10–13+36.
8. Liang, N.; Mao, J.; Yan, R.; Liu, X.; Zhou, X. Corrosion resistance of multiscale polypropylene fiber-reinforced concrete under sulfate attack. *Case Stud. Constr. Mater.* **2022**, *16*, e1065. [[CrossRef](#)]
9. Abousnina, R.; Premasiri, S.; Anise, V.; Lokuge, W.; Vimonsatit, V.; Ferdous, W.; Alajarmeh, O. Mechanical Properties of Macro Polypropylene Fibre-Reinforced Concrete. *Polymers* **2021**, *23*, 4112. [[CrossRef](#)]
10. Liang, N.; Geng, S.; Mao, J.; Liu, X.; Zhou, X. Investigation on cracking resistance mechanism of basalt-polypropylene fiber reinforced concrete based on SEM test. *Constr. Build. Mater.* **2024**, *411*, 134102. [[CrossRef](#)]
11. Gao, Y.; Zhou, B.; Yao, X.; Guan, J.; Han, X. The Influence of Metakaolin and Polypropylene Fiber Concrete on Mechanics Properties and Microstructure Combined Action under Multi-Salt Soaking and Freeze–Thaw. *Materials* **2023**, *16*, 5525. [[CrossRef](#)]
12. Ahmad, J.; BurduhosNergis, D.; Arbili, M.; Alogla, S.; Majdi, A. Deifalla Ahmed Farouk. A Review on Failure Modes and Cracking Behaviors of Polypropylene Fibers Reinforced Concrete. *Buildings* **2022**, *12*, 1951. [[CrossRef](#)]
13. Cui, K.; Xu, L.; Li, X.; Hu, X.; Huang, L.; Deng, F.; Chi, Y. Fatigue life analysis of polypropylene fiber reinforced concrete under axial constant-amplitude cyclic compression. *J. Clean. Prod.* **2021**, *319*, 128610. [[CrossRef](#)]
14. Gong, L.; Liang, Y.; Yu, X.; Du, Q. Damage Prediction of Hydraulic Concrete in Severe Cold Region Based on FOTP-GM (1, 1) Model. *KSCE J. Civ. Eng.* **2023**, *27*, 2993–3005. [[CrossRef](#)]
15. Li, G.; Yu, X.; Liang, Y.; Gong, X.; Du, Q. Multi-scale deterioration and microstructure of polypropylene fiber concrete by salt freezing. *Case Stud. Constr. Mater.* **2023**, *18*, e01762.
16. Al, L.; Khazaly, A.; Shabbar, R.; Jabal, Q.; Al, A. Effect of Polypropylene Fibers on some Mechanical Properties of Concrete and Durability against Freezing and Thawing Cycles. *Key Eng. Mater.* **2021**, *895*, 130–138.
17. Zhou, Z.; Zhang, J.; Shi, X.; Ban, J.; Yang, F. Research on frost and salt-frost resistance of polypropylene fiber concrete. *J. Water Resour. Water Eng.* **2014**, *25*, 152–155+160. (In Chinese)
18. Zhao, Z. Study on the Salt Frost Resistance of Polypropylene Fiber Concrete. Master’s Thesis, Xi’an University of Architecture and Technology, Xi’an, China, 2011.
19. Teng, F. *Study on Freezing-Thawing Damage Model of Polypropylene Fiber Concrete*; Hubei University of Technology: Wuhan, China, 2015; p. 6.
20. Gong, S.; Wang, T.; Hasan, M.; Mei, X.; Tan, Z.; Su, T.; Cao, F. Effect of polypropylene fiber and nano-silica on the compressive strength and frost resistance of recycled brick aggregate concrete. *Nanotechnol. Rev.* **2023**, *12*, 174. [[CrossRef](#)]
21. Tipu, R.K.; Panchal, V.R.; Pandya, K.S. An ensemble approach to improve BPNN model precision for predicting compressive strength of high-performance concrete. *Structures* **2022**, *45*, 500–508. [[CrossRef](#)]
22. Awolusi, T.F.; Oke, O.L.; Akinkulore, O.O.; Sojobi, A.O.; Aluko, O.G. Performance comparison of neural network training algorithms in the modeling properties of steel fiber reinforced concrete. *Heliyon* **2019**, *5*, e01115. [[CrossRef](#)]
23. Chen, G.; Zhu, D.; Wang, X.; Zhou, C.; Chen, X. Prediction of Concrete Compressive Strength Based on the BP Neural Network Optimized by Random Forest and ISSA. *J. Funct. Spaces* **2022**, *8*, 27. [[CrossRef](#)]
24. Tian, T.; Li, R. Research Progress of Predicting Concrete Strength Based on Artificial Neural Networks. *JRSE* **2021**, *3*, 8.
25. Tareq, S.; Hegazy, R.; Usama, I.; Siti, K.; Mohammad, A.; Abdul, G.; Malek, A. Boosting Biodiesel Production from Dairy-Washed Scum Oil Using Beetle Antennae Search Algorithm and Fuzzy Modelling. *Resources* **2023**, *12*, 131. [[CrossRef](#)]
26. Li, B.; Xu, Y.; Zhou, Q.; Gao, P.; Guo, X.; Liu, Z.; Jiang, H. Thermal Error Modeling of Numerical Control Machine Based on Beetle Antennae Search Back-propagation Neural Networks. *Int. J. Comput. Intell. Syst.* **2023**, *16*, 84.

27. Li, G.; Xue, Y.; Qu, C.; Qiu, D.; Wang, P.; Liu, Q. Intelligent prediction of rockburst in tunnels based on back propagation neural network integrated beetle antennae search algorithm. *Environ. Sci. Pollut. Res.* **2022**, *30*, 33960–33973. [[CrossRef](#)]
28. Sun, J.; Wang, J.; Zhu, Z.; He, R.; Peng, C.; Zhang, C.; Huang, J.; Wang, Y.; Wang, X. Mechanical Performance Prediction for Sustainable High-Strength Concrete Using Bio-Inspired Neural Network. *Buildings* **2022**, *12*, 65. [[CrossRef](#)]
29. Wen, J.; Miao, H.; Liu, X. Roughness Prediction in Deep Hole Based on BAS-BP. *Mach. Des. Res.* **2019**, *35*, 80–83. (In Chinese)
30. Wang, T.; Liu, Q. The assessment of storm surge disaster loss based on BAS-BP model. *Mar. Environ. Sci.* **2018**, *37*, 457–463. (In Chinese)
31. Xu, K.; Shen, C.; Xu, C.; Fan, L.; Huo, H.; Xu, J.; Kuang, X.; Cui, L. Modeling and control-oriented thermal characteristics under variable load of the solid oxide fuel cell. *J. Solid State Electrochem.* **2023**, *27*, 2083–2099. [[CrossRef](#)]
32. Tang, X.; Ma, J.; Zhou, S.; Shan, T. Parking Demand Prediction Method of Urban Commercial-Office Complex Buildings Based on the MRA-BAS-BP Algorithm. *J. Adv. Transp.* **2022**, *2022*, 2529912. [[CrossRef](#)]
33. Wang, S.; Liu, S.; Zhang, J.; Che, X.; Wang, Z. Deming Kong. Feasibility study on prediction of gasoline octane number using NIR spectroscopy combined with manifold learning and neural network. *Spectrochim. Acta A Mol. Biomol. Spectrosc.* **2020**, *228*, 117836. [[CrossRef](#)]
34. Xu, C.; Chen, J.; Li, Z.; Lian, H. Durability and strength prediction of fiber concrete under saline freezing condition. *Hydro-Sci. Eng.* **2024**, 94–103. (In Chinese) [[CrossRef](#)]
35. Zheng, L.; Zhou, J. Mechanical, Chloride Permeation, and Freeze–Thaw Resistance of Recycled Micronized Powder Polypropylene-Fiber-Engineered Cementitious Composites. *Buildings* **2023**, *13*, 2755. [[CrossRef](#)]
36. Thomoglou, A.K.; Falara, M.G.; Voutetaki, M.E.; Fantidis, J.G.; Tayeh, B.A.; Chalioris, C.E. Electromechanical properties of multi-reinforced self-sensing cement-based mortar with MWCNTs, CFs, and PPs. *Constr. Build. Mater.* **2023**, *400*, 132566. [[CrossRef](#)]

Disclaimer/Publisher’s Note: The statements, opinions and data contained in all publications are solely those of the individual author(s) and contributor(s) and not of MDPI and/or the editor(s). MDPI and/or the editor(s) disclaim responsibility for any injury to people or property resulting from any ideas, methods, instructions or products referred to in the content.